ELSEVIER

Contents lists available at ScienceDirect

Electrochimica Acta

journal homepage: www.journals.elsevier.com/electrochimica-acta





Electrochemical redox of arsenic (III) and Cu (II) mixtures with ultraflat Au (111) thin films in water

Tybur Q. Casuse-Driovínto ^{a, b}, Angelica Benavidez ^b, Noah Jemison ^b, José M. Cerrato ^{a, b}, Juan Feliu ^c, Fernando H. Garzón ^{b, *}

- a Gerald May Department of Civil, Construction & Environmental Engineering, 1 University of New Mexico, MSC01 1070, Albuquerque, NM 87131, USA
- b Center for Micro-Engineered Materials, University of New Mexico, 1001 University Blvd SE, Albuquerque, NM 87106, USA
- ^c Instituto de Electroquímica, Universidad de Alicante, Apdo. 99, E'0308, Alicante, Spain

ARTICLE INFO

Keywords:
Arsenic
Copper
Electrochemical detection
Gold single crystals
Gold Thin Films
Water

ABSTRACT

The ability to detect trace concentrations of arsenite, As (III), in real water solutions is impacted by cocontamination of other metals and co-occurring ions. The presence of copper (II) ions are the most likely cocontaminant in natural waters to interfere with electrochemical As (III) detection, due to the close oxidation potentials of Cu (II) and As (III). The use of well-oriented ultraflat Au(111) thin film electrodes provided increased peak separation and sensitivity for electrochemical deposition and oxidation of Cu (II) and As (III) in 0.5 M sulfuric acid compared to an Au wire electrode. However, mixtures of Cu (II) and As (III) altered the oxidation peak positions during both cyclic voltammetry (CV) and linear stripping voltammetry (LSV) analysis. Calibration curves using the standard additions method in trace concentrations were conducted for Cu, As, and Cu & As solutions. Sweeping the potential at 10 mV s⁻¹ during CV in Cu & As mixtures resulted in a sequential deposition condition where a layer of Cu inhibited co-deposition of As to the electrode. In contrast, the rapid potential stepping of LSV to a potential where Cu and As reduction simultaneously occurs produced a peak profile different from Cu or As alone. A larger oxidation peak during LSV was also observed when both Cu and As were present. X-ray photoelectron spectroscopy indicates a Cu-As alloy is formed on the surface after LSV deposition.

SYNOPSIS: Analysis of Cu (II), As (III) and Cu (II) & As (III) mixtures suggests that a Cu_3As intermetallic phase is formed during LSV which impacts trace As detection even in trace Cu conditions. This has important implications for the ability to determine As concentrations near the MCL of 10 μ g L^{-1} in natural water systems which may contain Cu (II) and other co-contaminants.

1. Introduction

The World Health Organization and United States Environmental Protection Agency considers $10~\mu g~L^{-1}$ of As (III) toxic and carcinogenic [1,2]. A considerable portion of the U.S. and global population obtain their daily drinking water directly from surface or groundwater sources which are not protected by municipal water treatment systems [3–5]. In several studies of private water wells in the United States, arsenic exceeded the EPA maximum contaminant limit (MCL) in 7–10 % of wells [6,7]. To minimize exposure, detection of toxic As(III) at trace concentrations is critical.

By quickly and inexpensively quantifying As (III) in the field, electrochemical methods are valuable for identifying unsafe As

concentrations and assessing remediation efficacy in natural water samples [8–10]. Techniques such as linear stripping voltammetry are proven to be accurate at part per billion (μ g L⁻¹) concentrations and are capable of detecting multiple co-occurring redox active species simultaneously. Electrochemical detection for heavy metals in water therefore can be a lifesaving, portable, and rapid tool for supporting community health [11–14]. Gold (Au) electrodes are the standard for electrochemical As detection due to their high nobility, reversible As (III) redox reaction, and broad region of stability [9,15–19]. Thin Au films, nanoparticles, and microarrays on a variety of substrates have been investigated to identify low-cost and highly effective electrode materials [20–26]. Recent works have identified controlled Au surface morphology as a potential path to increased sensitivity and selectivity

E-mail address: garzon@unm.edu (F.H. Garzón).

^{*} Corresponding author.

for As (III) detection [27-33].

The use of electrochemical sensors with gold electrodes for arsenic detection may be negatively affected by interferences, including copper. Arsenic is commonly mobilized into water with many other anions such as sulfate and cations such as uranium, lead, iron, and copper [34,35]. Copper (II) is the most commonly cited cation interference with electrochemical As (III) detection and is used as an example interferant to determine the selectivity of novel electrodes [32,36–39]. Several studies have identified the mechanisms for sulfate assisted electrochemical Cu (II) reduction and oxidation at Au(111) surfaces which contribute to a characteristic three peak cyclic voltammogram [40–44]. The formation of Cu-As alloys during deposition and overlapping oxidation peaks has previously impeded our group's ability to detect trace concentrations of As in the presence of high concentrations of Cu (II) [45,46].

The objective of this work is to assess the capability of a well-oriented and ultraflat Au(111) thin film, Au(UTF), to selectively detect As (III) in the presence of Cu (II). In this study, linear stripping voltammetry (LSV) and cyclic voltammetry (CV) were used to systematically identify the impacts of Cu (II) co-contamination on As (III) detection using a Au(UTF) in multiple Cu(II) and As(III) concentration mixtures

2. Experimental

2.1. Materials Description and Characterization

Ultraflat Au(111) Thin Film. Ultraflat Au(111) thin films, Au(UTF), were obtained from Platypus Technologies and have thickness of approx. 100 nm. The average grain area is 3.64 \pm 0.2 μ m² with predominantly Au(111) surface orientation. A new Au(UTF) electrode was used for each experiment. A CV from 0.7 to 1.7 V vs. RHE at 10 mV s⁻¹ was performed at the begginning of each experiment to assess surface orientation and electrochemical surface area for current density normalization of the Au(UTF) and Au(Wire) electrodes. As can be seen in Figure S1, the Au(UTF) surface oxidation begins with a shoulder in the positive sweep direction beginning at 1.4 V which leads to a single sharp peak at 1.6 V. This demonstrates that the Au surface is predomininantly Au(111) oriented as compared to the Au(Wire) electrode which presents a broad set of peaks from 1.4 to 1.6 V for Au oxidation indicating multiple surface orientations [47]. The area of the Au reduction peak occuring at 1.2 V was determined and a value of 660 μC cm⁻² was used to normalize experimental results. The reference value used represents a three-electron transfer process per Au(111) surface atom with a specific current of 220 µC cm⁻² per electron.

2.2. Electrochemical characterization

Electrochemical experiments were carried out in a 200 ml five port glass cell, using an Au wire as a counter electrode and a reversible hydrogen electrode (RHE) as a reference electrode with a fritted glass tube to separate the RHE from the solution. Voltammetric experiments were carried out at room temperature using a PalmSens 4 PALM-PS4. F2.05 portable potentiostat. The potentiostat uses digital circuitry, and signal smoothing, similar to most modern potentiostats. Our groups previous studies using the Au(UTF) thin films showed lower detection limits and smaller linear regions [48]. This study may be different due to a change in potentiostat type, electrode shape, or vessel configuration. This variation is why we recommend electrode calibration via known additions or other methods to confirm the linearity of analysis via stripping voltammetry. Linear stripping voltammetry experiments contained an initial equilibrium step at 0.7 V, a deposition step for 60 s at 0 V and a sweep from 0 to 0.7 V at 10 mV s⁻¹. Cyclic voltammetry for analysis of Cu and As was swept between 0.7 and 0 V beginning in the negative direction. All solutions were made using ultrapure water (18.2 $M\Omega$ cm, Elga PureLab OptionQ), concentrated sulfuric acid (VWR, 95 wt %), As_2O_3 salt (Merck), and $CuSO_4$ salt. A 75 mg L^{-1} (10^{-1} M) As (III) in

 $0.5~M~H_2SO_4$ solution was used with to perform standard addition of As for trace As (III) detection and experiments. A 1 g L $^{-1}$ (1.57 mM) Cu (II) solution was prepared and used as the stock solution for standard additions of Cu(II). Standard additions were performed for 5, 10, 15, 25, 50, 75, 100, 125, and 175 μg L $^{-1}$ As (III) and 250, 500, 1000, and 1500 μg L $^{-1}$ Cu (II) in 0.5 M H $_2$ SO $_4$. The concentration of H $_2$ SO $_4$ as supporting electrolyte was maintained at 0.5 M for all electrochemical experiments and stock solutions. The scan rate for all experiments was maintained at 10 mV s $^{-1}$. For comparison of the Au(UTF) to a polycrystalline gold surface, the behavior of an Au(Wire) electrode was also studied in a 10 mg L $^{-1}$ Cu (II) solution.

2.3. Physical characterization

X-ray Photoelectron Spectroscopy. XPS measurements were performed using a Kratos Axis Ultra with a monochromatic Al $K\alpha$ source operating at 150 W (1486.6 eV). The operating pressure was 2×10^{-9} Torr. High-resolution spectra were acquired at a pass energy of 20 eV. XPS data was processed using Casa XPS software. To observe the Cu-As alloy in XPS the Au(UTF) electrode was placed in a 10 mg L⁻¹ Cu (II) & 750 $\mu g L^{-1}$ As (III) mixture in the typical three electrode setup used throughout our study. Only the deposition step of the LSV was performed; 60 s at 0 V vs. RHE. After deposition the electrode was quickly removed from the cell, rinsed with ultrapure water (less than 10 s), and inserted into the XPS system. The XPS system was prepped in the next room, so the transfer process was as fast as possible. Angle resolved XPS (ARXPS) was performed to obtain a depth profile of elemental composition. Decreasing the angle of beam entry results in increased beam interaction with the deposited surface layer. Therefore, changes in spectra for Cu and As during ARXPS are associated with variation in the adsorbed layer composition over the depth of the deposited film [49,50].

Thermodynamic Eh-pH Modelling. Arsenic and copper speciation and precipitation were modelled using the Geochemist's Workbench Rxn program [51] with Visual Minteq's thermodynamic database [52]. This database includes all major As(V), As(III), As(0), Cu(II), Cu(I), and Cu(0) species. Several Cu-As alloys (Cu₃As, Cu(AsO₂)₂, Cu₃AsO₄, and Cu₃(AsO₄)₂) were added to this database to determine their impact on Cu and As precipitation [53,54]. Cu and As speciation and precipitation was modelled at a Cu concentration of 1000 μ g L⁻¹, As concentration of 750 μ g L⁻¹, at 25 °C, a pH range of 0 to 14, and under the entire Eh range where water does not dissociate.

Statistical Analysis. Statistical analysis was performed in EXCEL to determine average and standard deviation of three consecutive measurements where applicable. The raw data was used to calculate the calibration plot of concentration vs. charge density. Limits of detection were determined using the equation LOD = (k * Sb)/m, where k was equal to 3 for a 98.3 % confidence level, Sb is the standard deviation for analysis of three blank curves, and m is the slope of the calibration curve.

3. Results & discussion

3.1. Increased sensitivity and selectivity for Cu & As at Au(UTF) compared to Au(wire) electrodes

Predominantly (111) oriented Au(UTF) electrodes were compared to polycrystalline Au wire electrodes, Au(Wire), for their sensitivity to Cu (II) and As (III) redox processes. Concentrations of 10 mg L $^{-1}$ Cu(II) or 750 µg L $^{-1}$ As (III) were used for this comparison. Fig. 1 presents CV studies between 0 and 0.7 V vs. RHE with a scan rate of 10 mV s $^{-1}$ starting in the negative direction. Table 1 contains charge and peak potentials for reduction and oxidation processes. Arsenic reduction and oxidation processes occur at lower potentials for the Au(UTF) electrode as compared to the Au(Wire) electrode (Fig. 1). The Au(UTF) also presents higher redox peak amplitude over baseline capacitive current than the Au(wire) electrode, which may be attributed to preferential

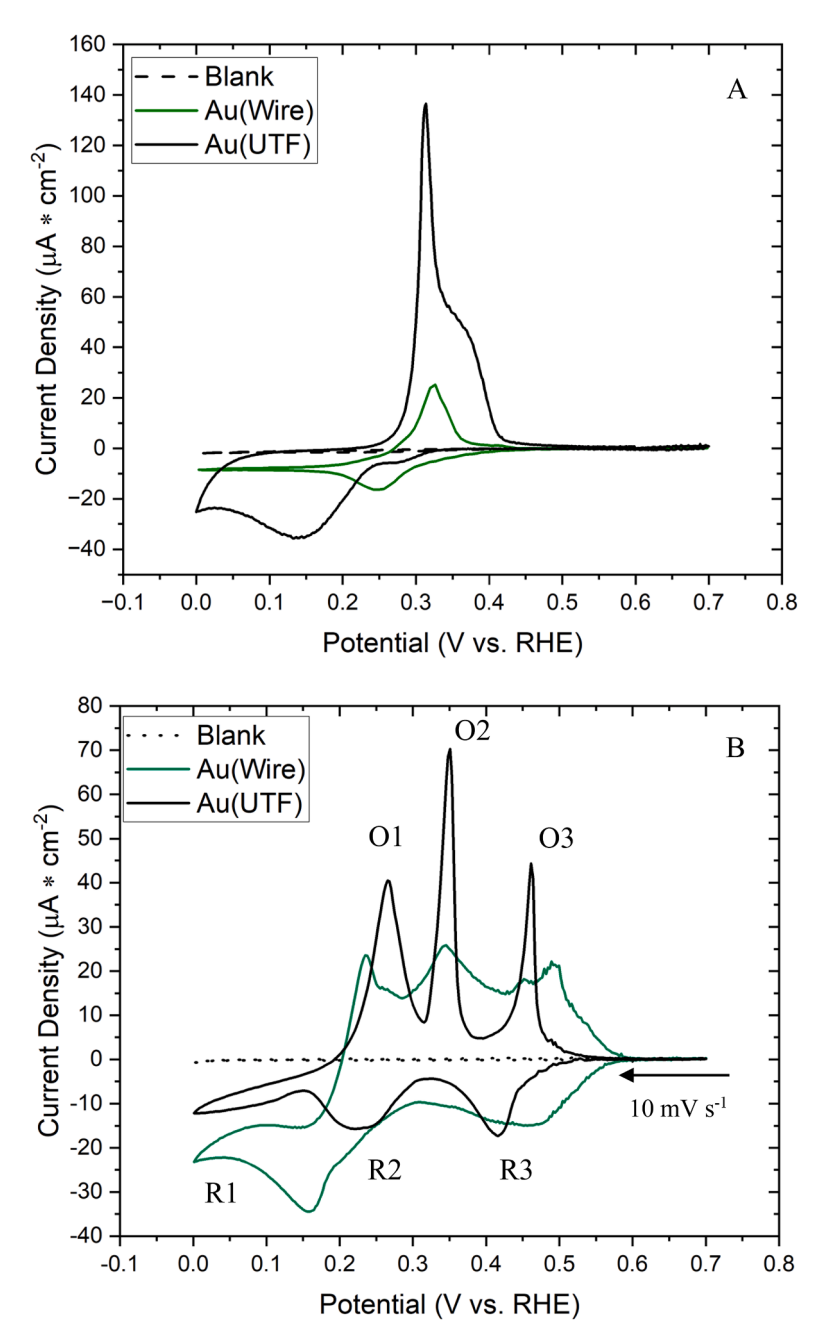


Fig. 1. Cyclic voltammograms comparing an ultraflat Au(111) thin film, Au(UTF), electrode compared to an Au wire, Au(Wire), electrode in A) 750 μ g L⁻¹ As (III) and B) 10 mg L⁻¹ Cu (II) with 0.5 M H₂SO₄ supporting electrolyte. Scan rate 10 mV s⁻¹; start in negative direction.

Table 1A Reduction and oxidation peak potentials during CV in 750 μ g L $^{-1}$ As (III) related to Fig. 1B.

Electrode	Reduction Peak Potential V vs. RHE	Oxidation Peak Potential V vs. RHE
Au(UTF)	0.15	0.31
Au (Wire)	0.25	0.33

orientation.

The behavior of the Au(UTF) and Au(Wire) electrodes were compared in a $10~\text{mg}~\text{L}^{-1}~\text{Cu}$ (II) solution. Copper redox reactions occurred at three separate potentials due to differences in adsorbed Cu structure formation on the Au(UTF) surface [41,55,56]. Each peak was

labeled for reference in the following analysis (Table 1B). Similar charge density for each reduction and oxidation process pair (O1 & R1, O2 & R2, O3 & R3) shows that the peaks are correlated and reversible. In previous studies on Cu redox at (111) oriented surfaces, peak pair R3 & O3 is often cited as the formation and dissolution of a 2/3 monolayer which is formed as a honeycomb structure on the Au(111) surface. Peak pair R2 & O2 is identified as the filling and dissolution of a 1:1 Cu to Au monolayer. Finally, peak pair R1 & O1 is associated with the formation of a bulk layer [56]. These peak pairs are relevant to discussion of CV studies. However, the oxidation peaks in LSV studies are taken to be indicators of the same processes. The combined charge for peaks O2 and O3 is 453 $\mu \text{C cm}^{-2}$. The sum of these two oxidation peaks aligns well with the expected specific current from a two-electron surface stripping process which could be associated with the formation of a full 1:1 monolayer of Cu at the Au(111) surface, 440 $\mu \text{C cm}^{-2}$. However, we

Table 1B Reduction and oxidation charge densities at the Au(UTF) electrode for three phase Cu redox peaks 1, 2, and 3 in $10 \, \mathrm{mg} \, \mathrm{L}^{-1}$ Cu (II) during cyclic voltammetry and linear stripping voltammetry.

Peak	Potential Range V vs. RHE	$\frac{CV}{\mu C}$ Reduction Charge Density $\mu C \ cm^{-2}$	Peak		Potential Range V vs. RHE	$\frac{CV}{\mu C}$ Oxidation Charge Density $\mu C \ cm^{-2}$	\underline{LSV} Oxidation Charge Density $\mu C \text{ cm}^{-2}$
R3	0.3- 0.6	185	03	0.46	0.4 - 0.6	183	151
R2	0.15 - 0.3	250	02	0.35	0.3 - 0.4 V	270	264
R1	0 - 0.15	286	01	0.25	0.2 - 0.3 V	275	338

observed that peak O3 accounts for only 2/5 of this charge instead of the expected 2/3 for the formation of a Cu honeycomb structure. This variance from expected ratios may be due to the presence of multiple randomly rotated Au(111) crystals with grain boundaries in the film resulting in various Au(111) terrace sizes [41]. However, the charge ratios may also be influenced by co-adsorbed sulfate [55,57]. The current density correlation to theoretical values and the ability to observe these processes in sharp and mostly separated peaks shows the quality of the Au(111) surfaces on the Au(UTF) for observing electrochemical processes with increased sensitivity and selectivity as shown in our previous studies [48].

The Au(UTF) presented better peak separation and sensitivity to each process as compared to the Au(Wire). The following experiments and data analysis are focused on results of studies with the Au(UTF), due to the focus of this study being on the impact of Au(111) surface orientation on detection of Cu and As.

3.2. Cu limitation of as deposition for Cu & As mixtures during cyclic voltammetry

Cyclic voltammetry studies in solutions containing both Cu and As were performed to provide detailed insights into the impacts of cooccurring Cu when electrochemically detecting As (III). We found that co-occurrence of Cu and As in solution limited the deposition of As (III). When 10 mg L^{-1} Cu (II) and 750 μ g L^{-1} As (III) were present in solution, the CV shows that the mixture resembled that of a CV in Cu alone more than As alone (Fig. 2). Copper deposition starts at roughly 0.2 V more positive (0.6 to 0.3 V) than As deposition (0.3 to 0 V), so a Cu layer may be forming on the Au surface prior to reaching a low enough potential for As deposition. This formation of a Cu layer inhibits the detection of a

peak at the predicted As deposition potential. However, the orientation and purity of the Cu film is unknown. We confirmed limited As deposition by comparing the charge passed during redox of the mixture and the individual analytes (Table 2). The charge associated with codeposition was not the sum of charge associated with Cu alone and As alone. Therefore, charge additive and independent deposition of Cu and As cannot be assumed.

3.3. Increased deposition and oxidation charge for Cu & as mixtures during linear stripping voltammetry

3.3.1. Studies with 10mg L^{-1} cu (II) & 750 $\mu\text{g L}^{-1}$ As (III) mixtures In contrast to CV studies, linear stripping voltammetry analysis of the

same solution conditions showed increased charges for mixtures as compared to individual analytes. Fig. 3A shows the LSV stripping peak for 10 mg L^{-1} Cu alone, 750 μ g L^{-1} As alone, and the 10 mg L^{-1} Cu & 750 $\mu g L^{-1}$ As mixture with a deposition time of 60 s at 0 V. The LSV analysis was performed directly after each CV study without removing

Total oxidation and reduction charge during CV at the Au(UTF) electrode in 750 μ g L⁻¹ As (III), 10 mg L⁻¹ Cu, and 750 μ g L⁻¹ As (III) + 10 mg L⁻¹ Cu mixture with 0.5 M H₂SO₄ supporting electrolyte.

Solution	Reduction Charge Density $\mu C \ cm^{-2}$	Oxidation Charge Density $\mu C \ cm^{-2}$
Blank (0.5 M H ₂ SO ₄)	34	3
$750~\mu g~L^{-1}~As$	752	710
$10~{ m mg~L}^{-1}~{ m Cu}$	788	613
$10{ m mg}{ m L}^{-1}{ m Cu}\&750{ m \mu g}$	960	727
L^{-1} As		

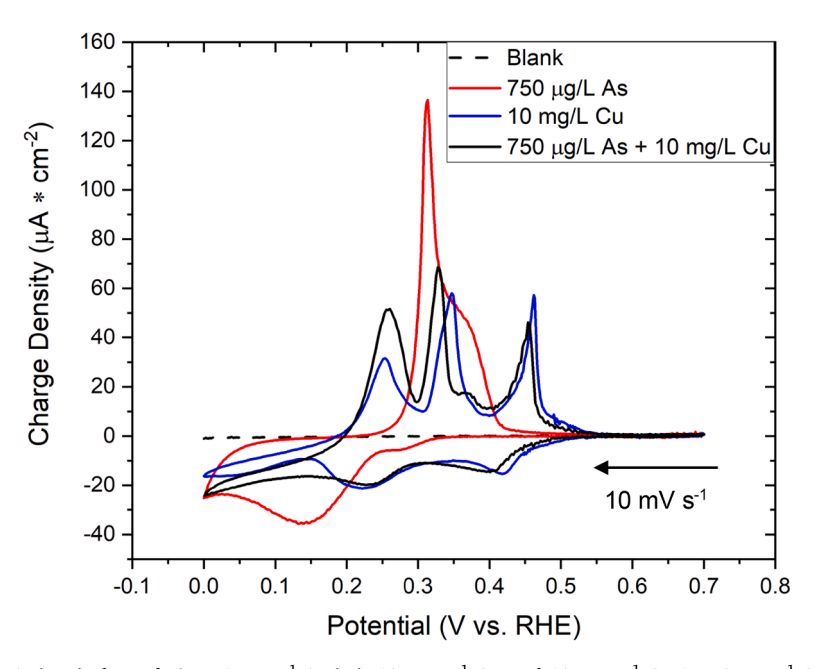
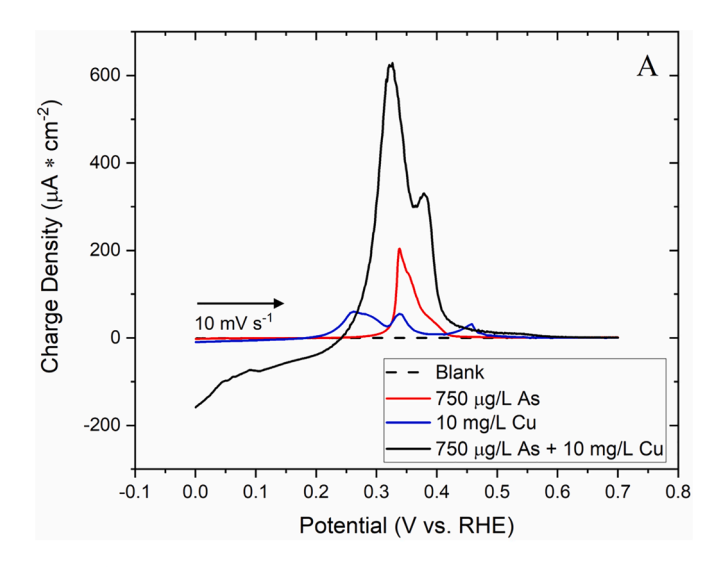


Fig. 2. Cyclic voltammetry at the Au(UTF) electrode in 750 μg L⁻¹ As (III), 10 mg L⁻¹ Cu, and 10 mg L⁻¹ Cu & 750 μg L⁻¹ As (III) mixture with 0.5 M H₂SO₄ supporting electrolyte. Scan rate 10 mV s⁻¹; start in negative direction.



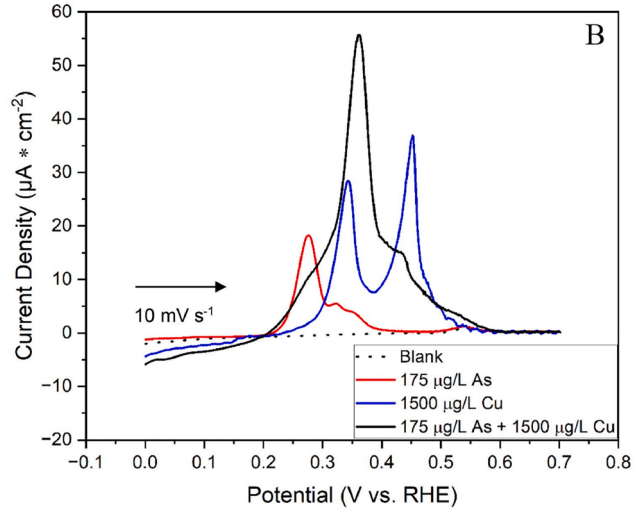


Fig. 3. Linear stripping voltammetry at the Au(UTF) electrode in A) 750 $\mu g \ L^{-1}$ As (III), 10 mg L^{-1} Cu, and 10 mg L^{-1} Cu (II) & 750 $\mu g \ L^{-1}$ As (III) mixture and **B)** 175 $\mu g \ L^{-1}$ As (III), 1500 $\mu g \ L^{-1}$ Cu (II), and 1500 $\mu g \ L^{-1}$ Cu (II) & 175 $\mu g \ L^{-1}$ As (III) mixture, with 0.5 M H_2SO_4 supporting electrolyte. Deposition for 60 s at 0 V vs. RHE and a scan rate of 10 mV s $^{-1}$.

the Au(UTF) electrode for consistency.

First, we discuss differences in LSV and CV studies for the individual analytes. The oxidation peak associated with bulk Cu dissolution (O1) was increased during LSV compared to CV in 10 mg $\rm L^{-1}$ Cu (II) (Table 1B). This may be due to more time spent below 0.15 V during LSV than CV, where bulk Cu formation is favorable. The higher potential peaks for Cu dissolution (O2 and O3) during LSV show lower current during LSV than CV. In solutions with As alone, LSV results in increased oxidation peak charge compared to CV experiments (Table 3). This

Table 3 Oxidation peak charge density during LSV for Au(UTF) in analysis of individual species and mixtures with $0.5~M~H_2SO_4$ supporting electrolyte.

Solution	Oxidation Charge Density $\mu C \ cm^{-2}$
Blank (0.5 M H ₂ SO ₄)	7
750 $\mu g L^{-1} As$	857
$10~{ m mg~L^{-1}~Cu}$	768
$10 \text{ mg L}^{-1} \text{ Cu \& 750 \mug L}^{-1} \text{ As}$	4921
$175~\mu g~L^{-1}~As$	125
1500 μg L^{-1} Cu	358
1500 μg L^{-1} Cu & 175 μg L^{-1} As	462

increase is likely due to more time in a potential region which is favorable for As deposition. The total width of the As detection peak is 100 mV, which is a small potential region compared to polycrystalline electrodes at similar concentrations of As, even when specialized pulse voltammetry techniques are utilized [9,15,17,32].

Here we discuss the differences between CV and LSV studies in cooccurring Cu (II) and As (III). When both 10 mg L $^{-1}$ Cu (II) and 750 μg L $^{-1}$ As (III) were present, LSV analysis resulted in a drastic increase in charge from 727 μC cm $^{-2}$ for CV to 4921 μC cm $^{-2}$ for LSV. This increase is higher than expected for an additive process where Cu and As were independently co-depositing at the Au surface. Additionally, the peak potential for the Cu and As mixture is 0.325 V with a shoulder peak at 0.375 V. Since the peak potentials do not align with the peak potential for Cu or As alone this result suggests a new intermetallic phase has been formed which is predicted by the Cu-As phase diagram [58–60]. Perhaps the increase in deposition charge is due to the suppression of parasitic reactions such as concurrent hydrogen evolution [61].

3.3.2. Studies with 1500 μ g L^{-1} Cu (II) and 175 μ g L^{-1} As (III)

Linear stripping voltammetry results are shown in Fig. 3B. The oxidation profile for Cu (II) alone shows two peaks at 0.35 V and 0.45 V. These oxidation peaks are associated with the dissolution of a monolayer surface structure. The lack of an oxidation peak at 0.25 V, when performing LSV in 1500 $\mu g \ L^{-1}$ Cu (II) alone, indicates that not enough Cu was deposited onto the surface during the deposition process to fill beyond a 1:1 monolayer. The peak for 175 $\mu g \ L^{-1}$ As (III) alone has a primary peak at 0.25 V with a shoulder at about 0.35 V. With both Cu and As in solution the predominant peak is at 0.36 V with shoulders on both sides. As an estimation, the oxidation charge during 1500 $\mu g \ L^{-1}$ Cu (II) alone would be equal to about 81 % of a monolayer, and the charge for 175 $\mu g \ L^{-1}$ As alone would correlate to about 19 % of a monolayer (Table 3).

3.4. Formation of Cu-As alloy

X-ray photoelectron spectroscopy (XPS) and thermodynamic modelling provide evidence that a Cu-As alloy is being formed during the deposition phase of LSV analysis. Fig. 4A presents elemental composition at 0, 20, 40 and 60° of sample tilt using angle resolved XPS analysis on the surface of the Au(UTF). The XPS analysis were conducted directly after deposition in a solution with co-occurring Cu & As. The elemental percentage of As increases from 6 to 18% elemental (8-26 wt %) as the angle of the film is tilted from 0 to 60°. This is shown by a decrease in the peak intensity for Cu while there was not as significant a change in the spectra for As during ARXPS (Figure S2). An increase in concentration with tilt angle indicates that As is more concentrated towards the surface of the adlayer than towards the Au(111) surface. This provides evidence that Cu may be forming a UPD layer initially and then subsequent layers include the formation of the Cu-As alloy. The concentration range determined is within the range where Cu₃As and other Cu-As alloys are formed according to metallurgical modelling [58-60].

Thermodynamic modelling for an aqueous electrolyte containing 0.5 M $\rm H_2SO_4, 1~mg~L^{-1}$ Cu (II), and 750 $\mu g~L^{-1}$ As (III) indicates that at the concentrations of interest Cu₃As is likely to be formed at a slightly higher potential than As alone (Fig. 4B). Although the thermodynamic characteristics of a bulk metal alloy are different from those in solution deposited thin films, the alloying phenomena cited in metallurgical studies may explain increased deposition and peak charge density for mixtures of 10 mg L^{-1} Cu (II) & 750 $\mu g~L^{-1}$ As (III) compared the individual species at the Au(UTF) surface during LSV [58,60]. A limitation of this study is that XPS and electrochemical data are not capable of discerning the structure of the intermetallic. Further studies using electron diffraction or atomic imaging are needed to determine if electrochemical deposition of the Cu-As intermetallic is forming a solid solution, or an ordered phase.

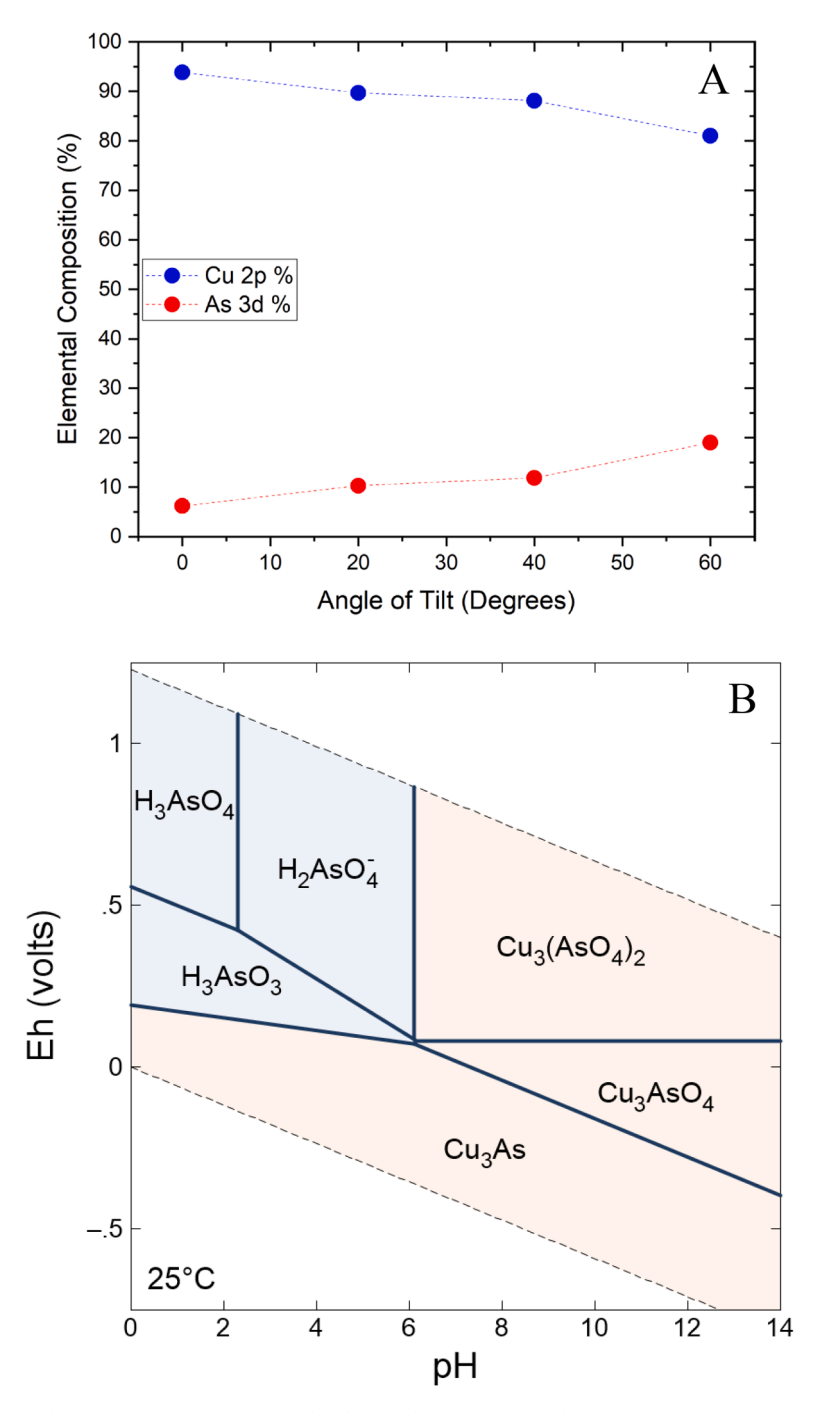


Fig. 4. A) Angle resolved X-ray photoelectron spectroscopy showing the elemental composition at the Au(UTF) surface after 60 s of deposition at 0 V vs. RHE in 10 mg L^{-1} Cu (II) and 750 μ g L^{-1} As (III) mixture B) Eh vs. pH diagram for 750 μ g L^{-1} As (III), 1 mg L^{-1} Cu (II) at 25 °C and 1.013 bars, generated using Geochemist's Workbench.

3.5. Co-occurrence of Cu limits selectivity for trace as detection

The Au(UTF) was highly effective at detecting Cu (II) alone near 1 mg L $^{-1}$ and trace concentrations of As (III) alone. The Au(UTF) was used to generate standard additions method calibration curves for 250, 500, 1000, and 1500 µg L $^{-1}$ (3.9, 7.9, 15.7 and 23.6 µM) Cu (II) as well as 5, 10, 15, 25, 50, 75, 100, 125, and 175 µg L $^{-1}$ (0.07, 0.13, 0.20, 0.33, 0.67, 1, 1.34, 1.67, and 2.3 µM) As (III), in 0.5 M H₂SO₄, Fig. 5A and C, respectively. Linear regression analysis showed that the adjusted R 2 for Cu (II) and As (III) detection were 0.901 and 0.999, respectively (Fig. 5B & D). This results in theoretical limits of detection (LOD) of 45 µg L $^{-1}$ (0.7 µM) Cu (II) alone and 0.6 µg L $^{-1}$ (0.01 µM) As (III) alone at the Au

(UTF) electrode. Sub part per billion detections of As (III) demonstrates accurate detection below the MCL while using LSV which is a method that can be automated and applied to a large set of electrodes.

The standard additions curves for trace As (III) alone presents three peaks associated with surface structure sensitive oxidation of As and sulfate. A small peak at 0.54 V, which is consistent throughout all curves including the blank, is commonly associated with the dissolution of an ordered sulfate layer at Au(111) electrode surfaces [62,63]. With incremental additions of As (III) to achieve between 5 and 25 $\mu g \ L^{-1}$, a peak with a bell shape increases at 0.35 V. However, at 50 $\mu g \ L^{-1}$ As (III) a second peak at 0.27 V begins to increase and eventually becomes the dominant peak at higher As (III) concentrations. The initial peak at 0.35

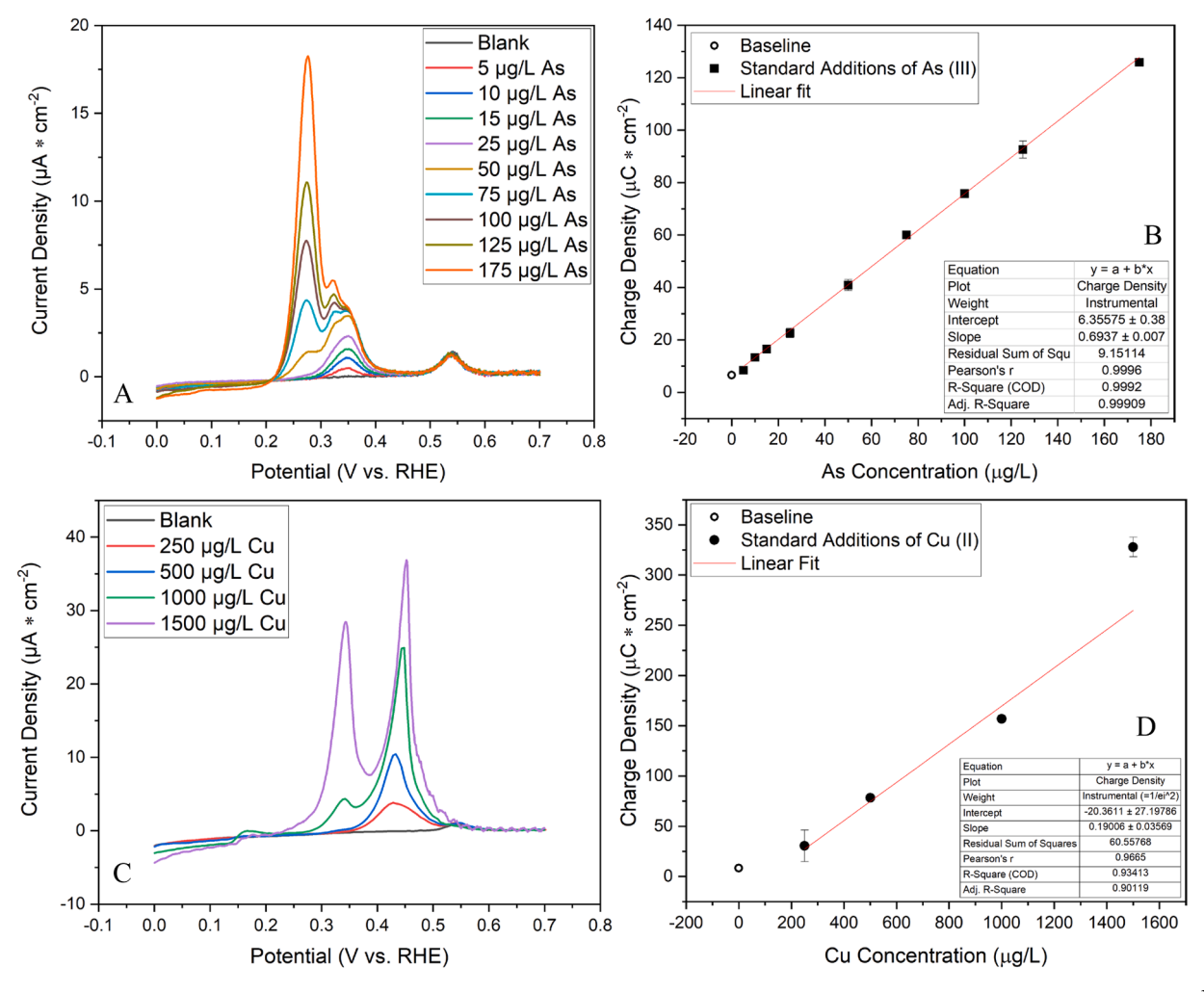


Fig. 5. Linear stripping voltammetry curves produced by standard additions method for trace detection of A) 5, 10, 15, 25, 50, 75, 100, 125, and 175 μ g L⁻¹ As (III) with B) associated As (III) calibration curve and C) 250, 500, 1000, and 1500 μ g L⁻¹ Cu (II) with D) associated Cu (II) calibration curve.

V becomes a shoulder and continues to have a maximum peak current near 6 μ A at concentrations above 50 μ g L $^{-1}$. This may be due to saturation of imperfections at the surface of the Au(UTF) which are not Au (111) oriented such as grain boundaries. Grain boundaries and other non (111) oriented surfaces may be adsorbing As (III) through underpotential deposition and thus require a higher potential to strip from the surface [48].

Concentrations of Cu alone from 250 to 1500 $\mu g \, L^{-1}$ Cu (II) show that increasing concentration results in two separate oxidation peaks. A peak at 0.45 V is present at 250 and 500 $\mu g \, L^{-1}$ Cu (II), and a second peak at 0.35 V is present as 1000 and 1500 $\mu g \, L^{-1}$ Cu(II) (Fig. 5C). This is consistent with previous sections showing that there is a maximal potential for the peak at 0.45 V due to the formation of an ordered submonolayer of Cu followed by the filling of a 1:1 monolayer at an Au (111) surface.

The Au(UTF) was used to generate curves for 5, 10, 15, 25, 50, 75, 100, 125, and 175 $\mu g \, L^{-1}$ As (III) in the presence of 1500 $\mu g \, L^{-1}$ Cu (II) (Fig. 6A & B). The initial peaks associated with 1500 $\mu g \, L^{-1}$ Cu (II) are at 0.34 and 0.45 V. With increasing As (III) concentrations the lower potential peak shifts from 0.34 to 0.37 V. The higher potential peak decreases in current from 37 to 19 μA and becomes a shoulder to the lower energy peak. The calibration curves show deviation from linearity was higher in the presence of Cu and As as indicated by a decrease in the residual sum of squares compared to As alone. The limit of detection for As (III) increased to 43.7 $\mu g \, L^{-1}$ (0.58 μM). The increased limit of detection effectively eliminates the ability to detect As at the maximum

contaminant level with 1500 $\mu g \; L^{-1}$ Cu (II) present [64].

Similar to the experiment above, the Au(UTF) was used to detect Cu standard additions of 250, 500, 1000, and 1500 $\mu g~L^{-1}$ Cu (II) in a solution containing 175 $\mu g~L^{-1}$ As (III) (Fig. 6C & D). Before Cu is added to solution there is a peak at 0.25 V, which is associated with 175 $\mu g~L^{-1}$ As (III). When 250 $\mu g~L^{-1}$ Cu (II) is added, the initial peak shifts positively to 0.3 V and a second peak at 0.44 V is introduced. Further additions of Cu (II) to 1500 $\mu g~L^{-1}$ continue to shift the lower potential peak to 0.35 V. The peak at 0.44 V also increases with increasing Cu concentration. This shows that concentrations as low at 250 $\mu g~L^{-1}$ Cu (II) can severely impact the peak shape and ability to detect trace As (III) at the Au(UTF) surface.

4. Conclusions

The results of this study demonstrated that the use of a highly oriented and ultraflat Au(111) surface provided increased sensitivity for Cu and As redox compared to polycrystalline electrodes. However, the Au (UTF) was not able to accurately detect As (III) in the presence of high concentrations of Cu (II) due to Cu-As alloy formation. The standard additions method was used to detect As (III) alone with a LOD of 0.6 μg L^{-1} in 0.5 M H_2SO_4 showing highly sensitive detection using a nanofilm of Au and the readily automatable LSV method. However, when 1500 μg L^{-1} Cu (II) was present the LOD was increased to 43.7 μg L^{-1} , making the electrode ineffective for detection at the 10 μg L^{-1} MCL for As (III).

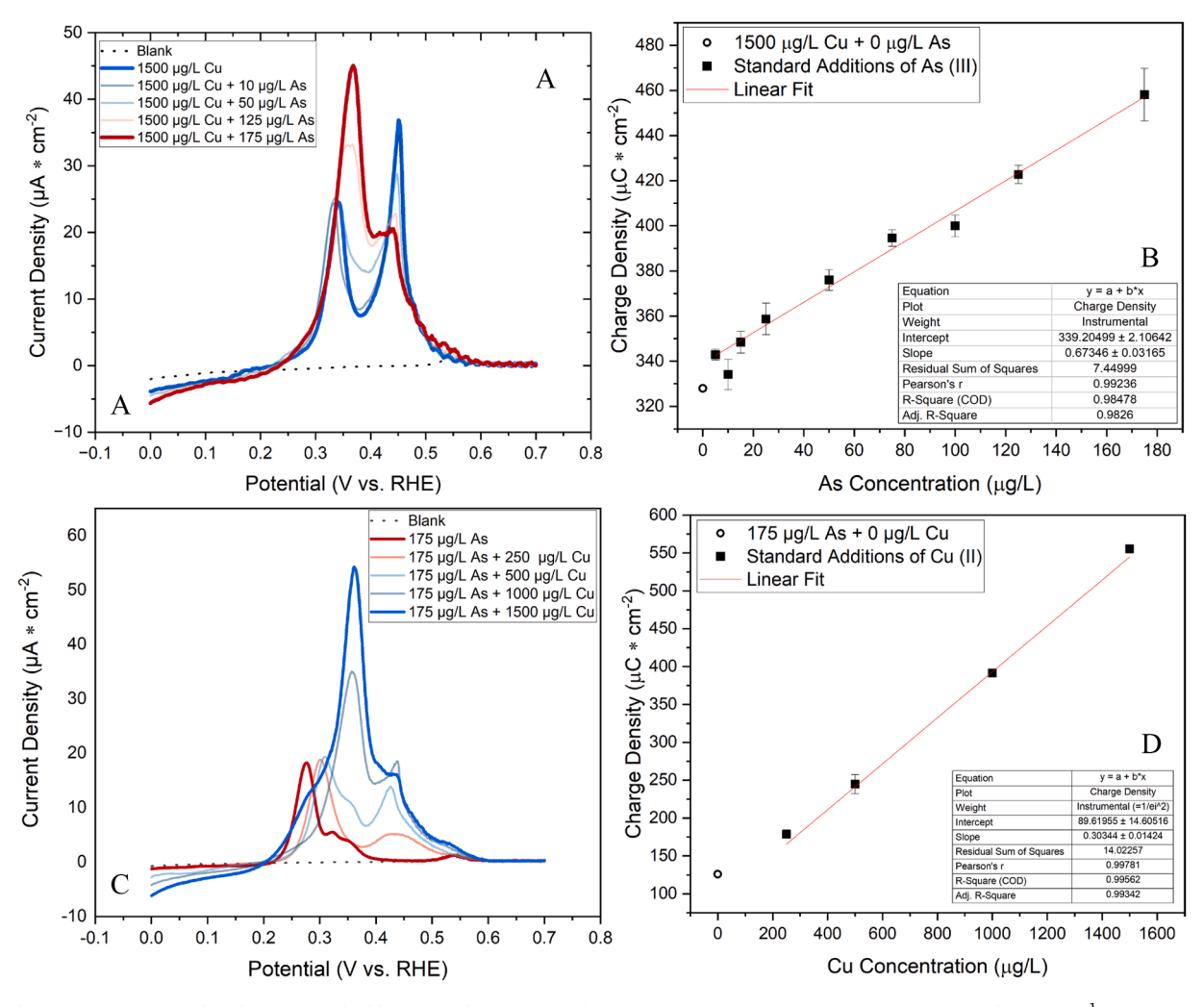


Fig. 6. Selected LSV curves produced by standard additions method for trace detection of **A**) 5, 10, 15, 25, 50, 75, 100, 125, and 175 μ g L⁻¹ As (III) to a solution containing 1500 μ g L⁻¹ Cu (II) with **B**) associated As (III) calibration curve, and **C**) 250, 500, 1000, and 1500 μ g L⁻¹ Cu (II) to a solution containing 175 μ g L⁻¹ As (III) with **D**) associated Cu (II) calibration curve.

sequential deposition of Cu then As lead to limited As deposition. However, when deposition is performed through LSV by a rapid step to a potential where both Cu and As are deposited there is an increase in oxidation peak charge density compared to Cu or As alone. At the concentrations studied, modelling illustrated that a stable Cu₃As species may be formed which is likely the cause for increased deposition when both Cu and As are present. This work provides insights into electrochemical Cu-As alloy formation on well-oriented Au(111) electrodes. Ultimately, our findings highlight the importance of Cu (II) removal before electrochemical analysis of As (III).

CRediT authorship contribution statement

Tybur Q. Casuse-Driovínto: Writing – original draft, Investigation, Formal analysis, Data curation. **Angelica Benavidez:** Writing – review & editing, Investigation, Formal analysis. **Noah Jemison:** Writing – review & editing, Investigation, Formal analysis. **José M. Cerrato:** Writing – review & editing, Supervision, Methodology, Funding acquisition, Formal analysis. **Juan Feliu:** Writing – review & editing, Methodology, Formal analysis. **Fernando H. Garzón:** Writing – review & editing, Writing – original draft, Supervision, Resources, Project administration, Formal analysis, Conceptualization.

Declaration of competing interest

The authors declare that they have no known competing financial interests or personal relationships that could have appeared to influence the work reported in this paper.

Data availability

Data will be made available on request.

Acknowledgments

This material is based upon work supported by the National Science Foundation (NSF) Graduate Research Fellowship Program (GRFP) under Grant No. (DGE-1418062), University of New Mexico Center for Water and the Environment, (NSF CREST Grant Number 1345169 and 1914490), the Center for Micro-Engineered Materials (NSF MRI Award 1828731), and the Army Research Office (ARO), Chemical Sciences Branch, Environmental Chemistry Research Area under contract W911NF-21–1–0249. Any opinion, findings, and conclusions or recommendations expressed in this material are those of the authors(s) and do not necessarily reflect the views of the National Science Foundation or the Army Research Office.

Supplementary materials

Supplementary material associated with this article can be found, in the online version, at doi:10.1016/j.electacta.2024.144220.

References

- [1] USEPA, Priority Pollutant List, 2014.
- [2] WHO, Arsenic Fact Sheet, World Health Organization, 2010.
- [3] A. Murray, A. Hall, J. Weaver, F. Kremer, Methods for estimating locations of housing units served by private domestic wells in the united states applied to 2010, JAWRA 57 (2021) 828–843.
- [4] Y. Bo, F. Zhou, J. Zhao, J. Liu, J. Liu, P. Ciais, J. Chang, L. Chen, Additional surfacewater deficit to meet global universal water accessibility by 2030, J. Clean. Prod. 320 (2021).
- [5] J. Podgorski, Global threat of arsenic in groundwater, Science 368 (2020) 845–850.
- [6] A.H. Welch, D. Westjohn, D.R. Helsel, R.B. Wanty, Arsenic in ground water of the United States: occurrence and geochemistry, Groundwater 38 (2000) 589–604.
- [7] M.A. Lombard, M.S. Bryan, D.K. Jones, C. Bulka, P.M. Bradley, L.C. Backer, M. J. Focazio, D.T. Silverman, P. Toccalino, M. Argos, Machine learning models of arsenic in private wells throughout the conterminous United States as a tool for exposure assessment in human health studies, Environ. Sci. Technol. 55 (2021) 5012–5023
- [8] J.C. Bullen, A. Torres-Huerta, P. Salaun, J.S. Watson, S. Majumdar, R. Vilar, D. J. Weiss, Portable and rapid arsenic speciation in synthetic and natural waters by an As(V)-selective chemisorbent, validated against anodic stripping voltammetry, Water Res. 175 (2020) 115650.
- [9] M. Kopanica, L. Novotný, Determination of traces of arsenic(III) by anodic stripping voltammetry in solutions, natural waters and biological material, Anal. Chim. Acta 368 (1998) 211–218.
- [10] S. Sikdar, M. Kundu, A review on detection and abatement of heavy metals, ChemBioEng Rev. 5 (2017) 18–29.
- [11] J. Das Joyati, P. Sarkar, J. Panda, P. Pal, Low-cost field test kits for arsenic detection in water. J. Environ. Sci. Health., A 49 (2014) 108–115.
- [12] J. Thangphatthanarungruang, A. Lomae, O. Chailapakul, S. Chaiyo, W. Siangproh, A low-cost paper-based diamond electrode for trace copper analysis at on-site environmental area, Electroanalysis 33 (2020) 226–232.
- [13] K.D. Reid, F. Goff, D.A. Counce, Arsenic concentration and mass flow rate in natural waters of the Valles caldera and Jemez Mountains region, New Mexico, N. M. Geol. 25 (2003) 75–82.
- [14] P.L.K. Smedley, D.G. Kinniburgh, A review of the source, behaviour and distribution of arsenic in natural waters, Appl. Geochem. 17 (2002) 517–568.
- [15] X. Dai, O. Nekrassova, M.E. Hyde, R.G. Compton, Anodic stripping voltammetry of arsenic(III) using gold nanoparticle-modified electrodes, Anal. Chem. 76 (2004) 5924–5929.
- [16] X. Dai Xuan, G.G. Wildgoose, C. Salter, A. Crossley, R.G. Compton, Electroanalysis using macro-, micro-, and nanochemical architectures on electrode surfaces. Bulk surface modification of glassy carbon microspheres with gold nanoparticles and their electrical wiring using carbon nanotubes, Anal. Chem. 78 (2006) 6102–6108.
- [17] L. Xiao, G.G. Wildgoose, R.G. Compton, Sensitive electrochemical detection of arsenic (III) using gold nanoparticle modified carbon nanotubes via anodic stripping voltammetry, Anal. Chim. Acta 620 (2008) 44–49.
- [18] F.T. Henry, Determination of trace level arsenic (III), arsenic(V), and total inorganic arsenic by differential pulse polarography, Anal. Chem. 51 (1979) 215–218
- [19] G. Forsberg, J.W. Olaughlin, R.G. Megargle, S.R. Koirtyohann, Determination of arsenic by anodic-stripping voltammetry and differential pulse anodic-stripping voltammetry, Anal. Chem. 47 (1975) 1586–1592.
- [20] L. Bu, J. Liu, Q. Xie, S. Yao, Anodic stripping voltammetric analysis of trace arsenic (III) enhanced by mild hydrogen-evolution at a bimetallic Au–Pt nanoparticle modified glassy carbon electrode, Electrochem. Commun. 59 (2015) 28–31.
- [21] A. Buffa, D. Mandler, Arsenic(III) detection in water by flow-through carbon nanotube membrane decorated by gold nanoparticles, Electrochim. Acta 318 (2019) 496–503.
- [22] E. Nunez-Bajo, M.C. Blanco-Lopez, A. Costa-Garcia, M.T. Fernandez-Abedul, Electrogeneration of gold nanoparticles on porous-carbon paper-based electrodes and application to inorganic arsenic analysis in white wines by chronoamperometric stripping, Anal. Chem. 89 (2017) 6415–6423.
- [23] Z.G. Liu, X.J. Huang, Voltammetric determination of inorganic arsenic, TrAC Trends in Analytical Chemistry 60 (2014) 25–35.
- [24] D. Kato, T. Kamata, D. Kato, H. Yanagisawa, O. Niwa, Au nanoparticle-embedded carbon films for electrochemical As(3+) detection with high sensitivity and stability, Anal. Chem. 88 (2016) 2944–2951.
- [25] Y. Song, G.M. Swain, Total inorganic arsenic detection in real water samples using anodic stripping voltammetry and a gold-coated diamond thin-film electrode, Anal. Chim. Acta. 593 (2007) 7–12.
- [26] H.B. Hu Haibing, H. Hu, B. Xie, Y. Lu, J. Zhu, Advances in electrochemical detection electrodes for As(III), Nanomaterials 12 (2022) 781.
- [27] X. Jiang, J. Ma, G. Jiang, M. Xu, X. Huang, G. Gao, X. Dai, Preparation of gold nanoplates using ortho carbonyl compounds as capping agents for electrochemical sensing of lead ions, Nanoscale Res. Lett. 16 (2021) 57.

- [28] Z. Jia, A.O. Simm, X. Dai, R.G. Compton, The electrochemical reaction mechanism of arsenic deposition on an Au(111) electrode, J. Electroanal. Chem. 587 (2006) 247–253.
- [29] D.D. Han, S.S. Li, Z. Guo, X. Chen, J.H. Liu, X.J. Huang, Shape dependent stripping behavior of Au nanoparticles toward arsenic detection: evidence of enhanced sensitivity on the Au (111) facet, RSC Adv. 6 (2016) 30337–30344.
- [30] B. Ren, L.A. Jones, M. Chen, D.K. Oppedisano, D. Qiu, S.J. Ippolito, S.K. Bhargava, The effect of electrodeposition parameters and morphology on the performance of Au nanostructures for the detection of As (III), J. Electrochem. Soc. 164 (2017) H1121–H1128.
- [31] N.U. Babar, K.S. Joya, M.A. Tayyab, M.N. Ashiq, M. Sohail, Highly sensitive and selective detection of arsenic using electrogenerated nanotextured gold assemblage, ACS Omega 4 (2019) 13645–13657.
- [32] Y. Zhang, D. Li, R.G. Compton, Arsenic (III) detection with underpotential deposition and anodic stripping voltammetry, ChemElectroChem 8 (2021) 3707–3715.
- [33] M.J.S. Kanido Camerun Kastro, Hwakyeung Jeong, Joongwon Kim, Effect of nanostructures of Au electrodes on the electrochemical detection of As, J. Electrochem. Sci. Technol (2019).
- [34] J.M. Blake, S. Avasarala, K. Artyushkova, A.-M.S. Ali, A.J. Brearley, C. Shuey, W. P. Robinson, C. Nez, S. Bill, J. Lewis, C. Hirani, J.S.L. Pacheco, J.M. Cerrato, Elevated concentrations of U and Co-occurring metals in abandoned mine wastes in a Northeastern Arizona Native American community, Environ. Sci. Technol. 49 (2015) 8506–8514.
- [35] C.W. Neil, Water chemistry impacts on arsenic mobilization from arsenopyrite dissolution and secondary mineral precipitation: implications for managed aquifer recharge, Environ. Sci. Technol. 48 (2014) 4395–4405.
- [36] B.K. Jena Bikash Kumar, C.R. Raj, Gold nanoelectrode ensembles for the simultaneous electrochemical detection of ultratrace arsenic, mercury, and copper, Anal. Chem. 80 (2008) 4836–4844.
- [37] S.B. Adeloju, T.M. Young, D. Jagner, G.E. Batley, Constant current cathodic stripping potentiometric determination of arsenic on a mercury film electrode in the presence of copper ions, Anal. Chim. Acta 381 (1999) 207–213.
- [38] X. Dai, R.G. Compton, Determination of copper in the presence of various amounts of arsenic with L-cysteine modified gold electrodes, Electroanalysis 17 (2005) 1835–1840.
- [39] N. Yogarajah Nevetha, N. Yogarajah, S.S.H. Tsai, Detection of trace arsenic in drinking water: challenges and opportunities for microfluidics, Environ. Sci. Water Res. Technol. 1 (2015) 426–447.
- [40] A. Moreira, A.V. Benedetti, P. Cabot, P. Sumodjo, Electrochemical behaviour of copper electrode in concentrated sulfuric acid solutions, Electrochim. Acta 38 (1993) 981–987.
- [41] A. Kuzume, E. Herrero, J.M. Feliu, R.J. Nichols, D.J. Schiffrin, Copper underpotential deposition at high index single crystal surfaces of Au, J. Electroanal. Chem. 570 (2004) 157–161.
- [42] E. Herrero, S. Glazier, L.J. Buller, H.D. Abruña, X-ray and electrochemical studies of Cu upd on single crystal electrodes in the presence of bromide: comparison between Au(111) and Pt(111) electrodes1Dedicated to Professor W. Vielstich on the occasion of his 75th birthday.1, J. Electroanal. Chem. 461 (1999) 121–130.
- [43] L. Blum, D.A. Huckaby, Underpotential deposition of Cu on Au(111): implications of the HB model, J. Electroanal. Chem. 375 (1994) 69–77.
- [44] P. Vélez, A. Cuesta, E.P.M. Leiva, V.A. Macagno, The underpotential deposition that should not be: $cu(1\times1)$ on Au(111), Electrochem. Commun. 25 (2012) 54–57.
- [45] X.X. Dai, X. Dai, R.G. Compton, Detection of As(III) via oxidation to As(V) using platinum nanoparticle modified glassy carbon electrodes: arsenic detection without interference from copper, Analyst 131 (2006) 516–521.
- [46] P. Vanysek, Electrochemical series, CRC Handbook Chem. Phys. 8 (2000).
- [47] A. Hamelin, Cyclic voltammetry at gold single-crystal surfaces. Part 1. Behaviour at low-index faces, J. Electroanaly. Chem. 407 (1996) 1–11.
- [48] T.Q. Casuse-Driovínto, R. Rizo, A. Benavidez, A.J. Brearley, J.M. Cerrato, F. H. Garzon, E. Herrero, J.M. Feliu, Increased sensitivity and selectivity for As(III) detection at the Au(111) surface: single crystals and ultraflat thin films comparison, J. Phys. Chem. C 126 (2022) 20343–20353.
- [49] L.Y. Chen Ly, L.Y. Chen, R.W. Hoffman, Angle-resolved x-ray photoelectronspectroscopy method for the thickness measurement of metal-oxide metal ultrathin films, Journal of Vacuum Science and Technology A 11 (1993) 2303–2307.
- [50] Z.S. He Zongsheng, Z. He, Z. Li, X. Jiang, C. Wu, Y. Liu, X. Song, Z. Yu, Y. Wang, Z. Lan, K. Sun, Surface investigation of Ni81Fe19 thin film: using ARXPS for thickness estimation of oxidation layers, Metals 11 (2021) 2061.
- [51] C. Bethke, B. Farrell, S. Yeakel, GWB reaction modeling guide, The Geochemists Workbench Release, 5 (2005).
- [52] J. Gustafsson, Visual Minteq ver. 3.0, KTH, Stockholm, 2012.
- [53] I. Barin, G. Platzki, Thermochemical Data of Pure Substances, Wiley Online Library, 1989.
- [54] B. Kasenov, S. Edil'baeva, S. Kasenova, A. Isabaev, M. Zhambekov, Evaluation of thermodynamic functions of arsenites and bismuthites of alkali, alkaline-earth, and some 3d and 4f transition metals, Russian J. Phys. Chem. A 72 (1998) 311–314.
- [55] Z. Shi, S. Wu, J. Lipkowski, Coadsorption of metal atoms and anions: Cu UPD in the presence of SO42-, Cl- and Br-, Electrochim. Acta 40 (1995) 9-15.
- [56] B. Madry, K. Wandelt, M. Nowicki, Deposition of copper multilayers on Au(111) in sulfuric acid solution: an electrochemical scanning tunneling microscopy study, Surf. Sci. 637-638 (2015) 77–84.
- [57] Z. Shi, J. Lipkowski, Coadsorption of Cu^{2+} and SO42— at the Au (111) electrode, J. Electroanal. Chem. 365 (1994) 303–309.
- [58] M. Mödlinger, R. de Oro Calderon, R. Haubner, Arsenic loss during metallurgical processing of arsenical bronze, Archaeol. Anthropol. Sci. 11 (2019) 133–140.

- [59] D. Shishin, E. Jak, Critical assessment and thermodynamic modeling of the Cu-As system, Calphad 60 (2018) 134–143.
- [60] O. Teppo, P. Taskinen, Assessment of the thermodynamic properties of arsenic-copper alloys, Scandinavian J. Metallurgy 20 (1991) 141–148.
 [61] J.A. Gauthier, L.A. King, F.T. Stults, R.A. Flores, J. Kibsgaard, Y.N. Regmi, K. Chan,
- [61] J.A. Gauthier, L.A. King, F.T. Stults, R.A. Flores, J. Kibsgaard, Y.N. Regmi, K. Chan T.F. Jaramillo, Transition metal arsenide catalysts for the hydrogen evolution reaction, J. Phys. Chem. C 123 (2019) 24007–24012.
- [62] Y. Fang, S.Y. Ding, M. Zhang, S.N. Steinmann, R. Hu, B.W. Mao, J.M. Feliu, Z. Q. Tian, Revisiting the atomistic structures at the interface of Au(111) electrode-sulfuric acid solution, J. Am. Chem. Soc. 142 (2020) 9439–9446.
- [63] B. Madry, K. Wandelt, M. Nowicki, Deposition of copper and sulfate on Au(1 1 1): new insights, Appl. Surf. Sci. 388 (2016) 678–683.
- [64] USEPA, Method 7063: arsenic in aqueous samples and extracts by anodic stripping voltammetry (ASV), 1996.